

# Predictions of homogeneous nucleation rates for $n$ -alkanes accounting for the diffuse phase interface and capillary waves

Barbora Planková,<sup>1, 2, a)</sup> Václav Vinš,<sup>1</sup> and Jan Hrubý<sup>1</sup>

<sup>1)</sup>*Institute of Thermomechanics of the CAS, v. v. i., Dolejškova 5, 182 00 Prague, Czech Republic*

<sup>2)</sup>*Department of Mathematics, Faculty of Nuclear Sciences and Physical Engineering, Czech Technical University in Prague, Trojanova 13, 120 00 Prague, Czech Republic*

(Dated: 20 June 2019)

Homogeneous droplet nucleation has been studied for almost a century but has not yet been fully understood. In this work, we used the density gradient theory (DGT) and considered the influence of capillary waves (CW) on the predicted size-dependent surface tensions and nucleation rates for selected  $n$ -alkanes. The DGT model was completed by an equation of state (EoS) based on the perturbed-chain statistical associating fluid theory (PC-SAFT) and compared to the classical nucleation theory and the Peng–Robinson EoS. It was found that the critical clusters are practically free of CW because they are so small that even the smallest CW wavelengths do not fit into their finite dimensions. The CW contribute to the entropy of the system and thus decrease the surface tension. A correction for the effect of CW on the surface tension is presented. The effect of the different EoSs is relatively small because by a fortuitous coincidence their predictions are similar in the relevant range of critical cluster sizes. The difference of the DGT predictions to the classical nucleation theory computations is important but not decisive. Of the effects investigated, the most pronounced is the suppression of the CW which causes a sizable decrease of the predicted nucleation rates. The major difference between experimental nucleation rate data and theoretical predictions remains in the temperature dependence. For normal alkanes, this discrepancy is much stronger than observed, e.g., for water. The theoretical corrections developed here have a minor influence on the temperature dependency. We provide empirical equations correcting the predicted nucleation rates to values comparable with experiments.

PACS numbers: 64.60.Q-, 64.60.qj, 82.60.Nh

---

<sup>a)</sup>Electronic mail: barbora.plankova@gmail.com

## I. INTRODUCTION

Description of homogeneous droplet nucleation is important in many natural and industrial processes such as formation of secondary aerosols in the atmosphere, formation of water droplets in the steam turbines, or nucleation during the gas-cleaning procedures, e.g., in processing of natural gas.

Despite many attempts that resolved partial subproblems of the nucleation, there is no complete theory which would give quantitatively correct predictions. The basic approach to the nucleation is through the classical nucleation theory (CNT), developed by Becker and Döring<sup>1</sup> and extended by Zeldovich.<sup>2,3</sup> Its main core is to model a droplet as a pure liquid cluster with a step-wise phase interface. However, the real thickness of the interface is comparable with the size of the droplets during the nucleation (in the range of nanometers). The CNT has been described in various textbooks.<sup>4-6</sup> In a review by Wyslouzil and Wölk published last year,<sup>7</sup> they discussed some recent developments in the CNT. Also last year Némec<sup>8</sup> presented a formulation of the CNT for bubble nucleation in binary solutions.

Unlike a zero thickness of the phase interface considered in CNT, a smooth change of the density between the two phases describes reality better. This approach is considered in the classical density functional theory (DFT) and its approximation, the density gradient theory (DGT). The DGT was first developed in pioneering work of van der Waals,<sup>9,10</sup> and later thoroughly elaborated by Cahn and Hilliard.<sup>11,12</sup> The DFT without the gradient simplification was proposed by Ebner<sup>13</sup> and developed by Evans<sup>14</sup>, based on the quantum DFT. DFT and DGT are widely used for the planar phase interfaces. Enders et al.<sup>15-18</sup> combined the DGT and the SAFT (Statistical Associating Fluid Theory) equation of state (EoS) for pure fluids and mixtures. More recently Fu et al.<sup>19,20</sup> used the DGT along with the perturbed chain (PC) modification of SAFT EoS for the surface tension calculations of CO<sub>2</sub> and hydrocarbons. Gross<sup>21</sup> and Klink and Gross<sup>22</sup> combined the DFT with PCP-SAFT, i.e., PC-SAFT extended for polar substances, EoS for pure fluids and mixtures. Recently, Klink et al.<sup>23</sup> applied DFT with PCP-SAFT EoS also to the liquid-liquid phase interfaces.

Concerning the spherical phase interfaces, there are numerous works as well. Laaksonen and Oxtoby<sup>24</sup> studied mixtures using a perturbed Lennard-Jones fluid. Wilemski and Li<sup>25</sup> investigated the DGT of droplets near the spinodal. Iwamatsu<sup>26</sup> and Iwamatsu and Okabe<sup>27</sup> studied cavities and bubbles using DGT. McGrath et al.<sup>28</sup> examined the nucleation of argon

using the CNT, DFT and Monte Carlo simulations. Obeidat et al.<sup>29</sup> combined DGT and SAFT EoS for methanol. Xu et al.<sup>30</sup> investigated bubble nucleation using dynamical DFT along with the PC-SAFT EoS. They used a modified steepest descent algorithm (called the string method) to calculate the minimal free energy path. Wilhelmssen et al.<sup>31,32</sup> used a cubic EoS for bubbles and droplets to investigate their thermodynamic stability and computed rigidity constants and surface tension of a droplet for the Lennard–Jones fluid. Dahms<sup>33</sup> used the DGT and cubic EoS for pentafluoroethane (R-125).

Besides the non-zero thickness, the interface is also disturbed by a thermal motion of molecules. These undulations are called the capillary waves (CW), described by Buff, Lovett and Stillinger.<sup>34</sup> CW were later investigated by many researchers, e.g. by Kayser<sup>35</sup> who calculated the increase in interfacial tension caused by cutting off some CW, Beysens and Robert<sup>36</sup> and Meunier<sup>37,38</sup> who combined the smoothly changing density approach with CW. Mecke, Dietrich and Napiórkowski<sup>39–41</sup> combined DFT and CW to form an effective Hamiltonian and surface tension depending on the wavenumber  $q$ . The conclusions of their theory led to rather wide discussion.<sup>42–46</sup> Chacón, Tarazona and Alejandre<sup>47–49</sup> performed Monte Carlo simulations of CW. They developed a method to determine Gibbs dividing surface in simulations. Boltachev and Baidakov<sup>50</sup> studied vapor-liquid interfaces of argon, thickness of the interface and the Tolman length.

In this work we address the problem of homogeneous droplet nucleation with DGT using PC-SAFT EoS and considering the effect of CW. For comparison, we add the theoretical results also for CNT and cubic Peng–Robinson (PR) EoS.

This article is organized as follows. In Sec. II we describe some basic relations concerning the nucleation. We connect the nucleation rate to the work needed to form the droplet, called the work of formation, in supersaturated vapor. In Sec. III we provide mathematical results of DGT to determine the density profiles that correspond to the work of formation of a cluster. In Sec. IV we describe the PC-SAFT EoS. In Sec. V we characterize impact of CW on the surface tension and a way of how to eliminate CW from the input of DGT. In Sec. VI we explain mathematical methods for the numerical solution equations defined in Sec. III. In Sec. VII we provide the resulting nucleation rates of the four  $n$ -alkanes,  $n$ -heptane,  $n$ -octane,  $n$ -nonane and  $n$ -decane and compare them to the experimental data. We reevaluate the data to determine the temperature dependence of the supersaturation and number of molecules in the cluster. We examine impact of CW on the surface tension and

the nucleation rate. In the last section, Sec. VIII, we draw conclusions about the nucleation rates, the temperature dependence and influence of CW.

## II. NUCLEATION RATES

Nucleation of droplets in a homogeneous vapor can occur if the vapor density  $\rho_V$  is greater than the density of saturated vapor  $\rho_{V\infty}$  at a given temperature  $T$ . Subscript  $\infty$  refers to the infinite curvature radius of the planar phase interface under the saturation conditions. The departure of the system from saturation is expressed in terms of supersaturation  $S$  defined as

$$S = \exp\left(\frac{\mu_V - \mu_\infty}{k_B T}\right), \quad (1)$$

where  $\mu_V$  is the chemical potential of the vapor phase,  $\mu_\infty$  is the chemical potential at saturation, which is equal for liquid and vapor phases, and  $k_B$  is the Boltzmann constant. If  $S > 1$ , the vapor becomes supersaturated. Supersaturated vapor is in a metastable state, i.e., it is stable with respect to small fluctuations but unstable with respect to large fluctuations, particularly in the form of clusters of the newly forming phase.<sup>6,51</sup> Homogeneous droplet nucleation is the process of formation of liquid droplets in the supersaturated vapor phase free of aerosol particles, impurities or solid walls. These droplets can be viewed as clusters of  $n$  molecules, referred as  $n$ -mers in this case. Microscopically, these clusters grow or shrink if a monomer joins or leaves a cluster. Condensation and evaporation of larger clusters (dimers, trimers etc.) is less probable except for strongly associate vapors. Of all the  $n$ -mers, the most important for nucleation is the so-called critical cluster with  $n_c$  molecules which has the same probability to grow as to shrink.<sup>1</sup> In terms of thermodynamics, this condition can be interpreted as an equality of chemical potential in the liquid core of the critical cluster and the chemical potential of the supersaturated vapor,

$$\mu_L(n_c) = \mu_V. \quad (2)$$

The number of droplets formed in a unit of volume per a unit of time is called the nucleation rate,  $J$ . Considering the chain of individual growth-shrink processes, it is possible to derive an expression for the nucleation rate in the form of a converging infinite sum,<sup>4-6</sup>

$$J = \left[ \sum_{n=1}^{\infty} \frac{1}{f_n C_n^{\text{eq}}} \right]^{-1}, \quad (3)$$

where  $f_n$  is the condensation rate, i.e., the number of monomers impacting on the surface of  $n$ -mer per unit of time; the sticking probability is taken as unity.  $C_n^{\text{eq}}$  is the equilibrium concentration of  $n$ -mers at given  $T$  and  $\mu_V$  in a system which is constrained in the way that growth over certain size  $n_{\text{max}}$  is prohibited. If  $n_{\text{max}}$  is substantially larger than the critical size  $n_c$ , its magnitude does not play any role. When no interactions between large clusters are considered, the limit of maximal size of a  $n$ -mer can be placed to infinity,<sup>4</sup> as adopted in Eq. (3). The constrained equilibrium concentrations enter the nucleation theory via the condition of detailed balance<sup>4,6</sup> stating that in the equilibrium all microscopic processes must have their time-mirrored counterparts which are equally probable. This condition allows for expression of the evaporation rate in terms of the condensation rate. The latter is given as

$$f_n = \nu A_n, \quad (4)$$

where  $A_n$  is the surface area of  $n$ -mer and  $\nu$  is the impingement rate of monomers per surface area. This is given by the kinetic theory of gases as<sup>4,6,52</sup>

$$\nu = C_1 \sqrt{\frac{k_B T}{2\pi M}}, \quad (5)$$

where  $C_1$  is the concentration of monomers and  $M$  is the molecular mass. The concentration  $C_n^{\text{eq}}$  can be expressed in terms of the work of formation  $\Delta\Omega_n$  of an  $n$ -mer as<sup>4,6</sup>

$$C_n^{\text{eq}} = \frac{1}{\vartheta} \exp\left(-\frac{\Delta\Omega_n}{k_B T}\right), \quad (6)$$

where  $\vartheta$  is the volume available for the translation of the cluster and attributes to the translational degrees of freedom of the cluster. The Boltzmann factor  $\exp(-\Delta\Omega_n/k_B T)$  can be interpreted as a probability of observing at least one  $n$ -mer in a region of volume  $\vartheta$  within an equilibrium system. The original Becker-Döring<sup>1</sup> choice was  $1/\vartheta = \rho_V$ , which, however, has been shown to affect the dependence of cluster concentrations on supersaturation in a theoretically unacceptable manner.<sup>53–56</sup> In this work, we adopt  $1/\vartheta = \rho_{V\infty}$ , corresponding to the correction by Courtney.<sup>57</sup> The CNT modification by Girshick and Chiu<sup>54</sup> corresponds to  $1/\vartheta = \rho_{V\infty} e^\theta$ , where  $\theta$  is the so-called dimensionless surface tension (variable consisting of the surface tension, liquid density and thermal energy  $k_B T$ ). The reasoning behind the Girshick-Chiu modification is that the expression for equilibrium concentration of clusters, Eq. (6), should hold down to monomers – provided that the dimensionless surface tension is size-independent. Here, however, we consider the size dependency and, therefore, this correction was not adopted.

As usual, the sum in Eq. (3) is approximated by an integral. The integrand is a function of  $n$  showing a sharp peak at  $n_c$ , which is due to the exponential part (the work of formation) in Eq. (6). Compared to that, the condensation rate varies modestly with  $n$  and, therefore, can be approximated as  $f_n \simeq f_{n_c}$ .<sup>4-6</sup> In a more refined treatment,  $1/f_n$  can be approximated as a linear function of  $n$  in the neighborhood of  $n_c$ . The proportional part cancels out upon the integration. The peaked function  $1/C_n^{\text{eq}}$  is then replaced by a Gaussian function and, integrated, yielding<sup>4-6</sup>

$$J = \frac{1}{\vartheta} A(n_c) \nu \mathcal{Z} \exp \left( -\frac{\Delta\Omega(n_c)}{k_B T} \right), \quad (7)$$

where  $\mathcal{Z}$  is Zeldovich factor defined as

$$\mathcal{Z} = \sqrt{-\frac{\Delta\Omega''(n_c)}{2\pi k_B T}} \simeq \frac{2}{\rho_{L,\infty}} \sqrt{\frac{\sigma_\infty}{k_B T}}. \quad (8)$$

In Eq. (8),  $\Delta\Omega''$  is the second derivative of the work of formation with respect to the number of molecules in the cluster, evaluated for the critical cluster,  $\Delta\Omega''(n_c) = \partial\Delta\Omega/\partial n(n_c)$ ,  $\rho_{L,\infty}$  is the liquid density and  $\sigma_\infty$  is the surface tension for the saturated state. The rightmost expression of the Zeldovich factor is an approximation based on CNT. Although different expressions will be used for  $\Delta\Omega$ , the Zeldovich factor can be kept in the classical form because it is rather insensitive to the modifications considered. With Eqs. (5) and (8), and using  $\vartheta$  corresponding to Courtney's correction,<sup>57</sup> nucleation rate given by Eq. (7) becomes

$$J = \frac{\rho_V \rho_{V\infty}}{\rho_{L\infty}} \sqrt{\frac{2\sigma_\infty}{\pi M}} \exp \left( -\frac{\Delta\Omega}{k_B T} \right). \quad (9)$$

The work of formation  $\Delta\Omega$  of the critical cluster can be expressed in terms of the Gibbsian thermodynamics of phase interfaces as

$$\Delta\Omega = \frac{1}{3} A_s \sigma, \quad (10)$$

where  $A_s = 4\pi r_s^2$  is the area of the surface of tension of the cluster and  $r_s$  is its radius. The surface of tension is defined by postulating the Young-Laplace equation in its standard form,<sup>4,51</sup>

$$\Delta p = \frac{2\sigma}{r_s}, \quad (11)$$

where  $\Delta p = p_L - p_V$  is the Laplace pressure. The work of formation is connected to the surface tension via

$$\Delta\Omega = \frac{16\pi}{3} \frac{\sigma^3}{\Delta p^2}. \quad (12)$$

We note that the Laplace pressure  $\Delta p$  for the critical cluster is related to supersaturation given by Eq. (1) through the equality defined in Eq. (2) and the EoS.

The work of formation for the CNT is obtained by substituting the flat-interface surface tension  $\sigma_\infty$  into Eq. (12). Inversely, if  $\Delta\Omega$  is known, this equation can be used to compute the (size dependent) surface tension for the critical cluster. Typically, further simplifications are employed in CNT. In particular, the compressibility of the liquid is neglected and the gas phase is assumed as an ideal gas. These simplifications were not employed in this work, the CNT work of formation was computed from the EoS.

### III. DENSITY GRADIENT THEORY (DGT)

The DGT operates with a density  $\rho$  smoothly changing throughout the phase interface. The local Helmholtz energy density is assumed<sup>11</sup> as a function of density and invariants of the spatial derivatives of density – the gradient squared  $(\nabla\rho)^2$ , and the Laplacian  $\nabla^2\rho$ . The Helmholtz energy is expanded in terms of these invariants around the Helmholtz energy of the homogeneous fluid  $f^0(\rho)$  which can be computed from an EoS in the region between saturated vapor and saturated liquid. We note that this region involves metastable vapor, metastable liquid, and the region between spinodals, which is unstable in the homogeneous case, but inside the phase interface it is stabilized by the density gradient. Retaining only linear terms in a Taylor expansion with respect to variables  $(\nabla\rho)^2$  and  $\nabla^2\rho$ , the Helmholtz energy density reads<sup>11,12,58</sup>

$$f(\rho, \nabla\rho, \nabla^2\rho) = f^0(\rho) + c_1(\rho, T)\nabla^2\rho + c_2(\rho, T)(\nabla\rho)^2 + \dots, \quad (13)$$

where  $c_1$  and  $c_2$  are Taylor coefficients. Using the Green (divergence) theorem, the second derivative  $\nabla^2$  in Eq. (13) can be substituted to the first derivative which leads to<sup>11</sup>

$$f(\rho) = f^0(\rho) + c(\rho, T) \cdot (\nabla\rho)^2 + \dots \quad (14)$$

In Eq. (14), the second term accounts for the inhomogeneity induced by the interface. Coefficient  $c = -\partial c_1/\partial\rho + c_2$  is called the influence parameter<sup>11</sup> and can be related to the direct correlation function.<sup>59</sup> In this work, it will be evaluated rather from the experimental data (as discussed below) and assumed as density-independent.



The work of formation of a droplet according to DGT can be expressed as a volume integral consisting of homogeneous and gradient parts,<sup>11,59</sup>

$$\Delta\Omega[\rho(r)] = \int_0^\infty \left[ \Delta\omega^0(\rho) + \frac{1}{2}c \left( \frac{d\rho}{dr} \right)^2 \right] 4\pi r^2 dr, \quad (15)$$

where  $r$  is the radial coordinate (the distance from the center of the droplet). Term  $\Delta\omega^0$  is the difference of the grand-potential density of the inhomogeneous system with respect to the homogeneous one at the same chemical potential (equal to the negative of vapor pressure  $p_V$ ),

$$\Delta\omega^0 = f^0 - \rho\mu_V + p_V. \quad (16)$$

We note that the work of formation, Eq. (15), is not a mere function of the density, but a *functional* since its value depends on the whole density profile  $\rho(r)$  and not just on the local value. The work of formation has a saddle point for the density profile corresponding to the so-called critical cluster; the work of formation of the critical cluster is minimal with respect to all the properties in the functional space except for density profile variations changing the size of the cluster (shifting the phase interface closer to or further from the center), for which it is maximal.<sup>51,53</sup> Setting the functional derivative of Eq. (15) equal to zero as a condition for the saddle point leads to an Euler–Lagrange equation<sup>12</sup>

$$\frac{d^2\rho}{dr^2} + \frac{2}{r} \frac{d\rho}{dr} = \frac{1}{c} \Delta\mu(\rho). \quad (17)$$

In Eq. (17),  $\Delta\mu = \mu^0(\rho) - \mu_V$  is the difference of chemical potential of a hypothetical homogeneous fluid at given local density  $\rho$  and the actual chemical potential. The actual chemical potential is everywhere equal to chemical potential of the homogeneous vapor phase. To solve the Euler–Lagrange equation, two boundary conditions are needed,<sup>12</sup>

$$\rho(r \rightarrow \infty) = \rho_V, \quad \frac{d\rho}{dr}(0) = 0. \quad (18)$$

Other important outputs of the DGT calculations are the excess number of molecules  $\Delta N$  and the surface tension of the saturated state  $\sigma_\infty$  (corresponding to the planar phase interface). The excess number of molecules is a difference of the number of molecules in a system containing a cluster to the number of molecules in a system of the same volume containing homogeneous vapor only. It can be computed as

$$\Delta N = \int_0^\infty [\rho(r) - \rho_V] 4\pi r^2 dr. \quad (19)$$

The surface tension of the saturated state can be obtained in a relation similar to Eq. (15),

$$\sigma_{\infty} = \int_{-\infty}^{\infty} \left[ \Delta\omega^0(\rho) + \frac{1}{2}c \left( \frac{d\rho}{dz} \right)^2 \right] dz, \quad (20)$$

where  $z$  is the coordinate perpendicular to the phase interface. Surface tension can also be obtained from experimental data; therefore, Eq. (20) can be used for computation of the (density-independent) influence parameter  $c$ .<sup>60</sup>

#### IV. PC-SAFT EQUATION OF STATE

In this work, DGT was combined with the PC-SAFT<sup>61,62</sup> EoS, which belongs to the family of modern SAFT-type equations of state being developed since 1990's.<sup>63–65</sup> The SAFT-type equations produce a qualitatively correct isotherm in the two-phase region, the so-called van der Waals loop. On the other hand, they provide remarkably good results for the liquid phase compared, e.g., to the cubic equations. As a consequence, the SAFT-type equations represent a convenient tool for modeling of vapor-liquid phase interfaces and for modeling nucleation of droplets and bubbles using DFT and DGT.

The SAFT-type equations of state are defined in the form of the Helmholtz energy, which is given as a sum of the ideal gas part  $F_{\text{id}}$  evaluated from the isobaric heat capacity of the ideal gas and the residual part  $F_{\text{res}}$  defined by the SAFT terms. An important advantage of the SAFT-type equations is that the residual part of the Helmholtz energy is expressed as a sum of individual contributions accounting for various types of intermolecular interactions,<sup>65</sup> e.g., the van der Waals attractions, Coulombic forces, or hydrogen bonds.<sup>64,65</sup> In PC-SAFT, the residual part consists of the hard chain contribution  $F_{\text{hc}}$  representing the reference fluid and the perturbation contribution  $F_{\text{disp}}$ . The hard chain contribution and the perturbation contribution are defined by a set of three molecular parameters: the segment number  $m$ , the segment diameter  $\sigma$ , and the energy parameter  $\epsilon/k_{\text{B}}$ . Values of these parameters are usually correlated to the saturation pressure and the liquid density.<sup>62</sup> Due to their reasonable physical basis and possibility of considering various contributions in  $F_{\text{res}}$ , the SAFT-type equations can be applied to a large variety of substances ranging from relatively simple components such as gases,  $n$ -alkanes or halogenated hydrocarbons<sup>66,67</sup> to polar substances,<sup>68,69</sup> polymers,<sup>70</sup> and associating fluids.<sup>65,71</sup> Consequently, these equations of state are becoming popular both in scientific and engineering applications.<sup>64,65</sup> Molecular

parameters  $m$ ,  $\sigma$  and  $\epsilon/k_B$  for selected  $n$ -alkanes used in this study were taken from the original work of Gross and Sadowski.<sup>62</sup>

## V. CAPILLARY WAVES

Thermal motion of molecules causes that the interface is not a smooth surface but it is rather disturbed by the capillary waves (CW).<sup>34</sup> We will use some results of the so-called mode-coupling theory developed by Meunier<sup>38</sup> which adds the effect of the broadening of the phase interface due to the CW to the surface tension of the planar phase interface.

We define a “bare” surface tension  $\sigma_{\text{bare}}$ , as the surface tension of a phase interface which is forced to be perfectly planar, cleared of CW. The bare surface tension still accounts for some thermal motion of molecules, which, however, is only correlated over a lengthscale comparable to the bulk correlation length. The surface tension determined in macroscopic experiments  $\sigma_{\text{exp}}$  includes the effect of CW. Allowing CW adds some disorder to the system. Consequently, the primary effect of CW is increasing the surface excess entropy and thus, in a product with temperature, reducing the surface tension as,<sup>38</sup>

$$\sigma_{\text{exp}} = \sigma_{\text{bare}} - \frac{3}{8\pi} k_B T q_{\text{max}}^2, \quad (21)$$

where  $q_{\text{max}}$  is the upper cutoff of the wavenumbers considered.  $q_{\text{max}}$  corresponds to CW with the smallest wavelength that are not already accounted for in DGT.

Meunier<sup>38</sup> estimated  $q_{\text{max}}$  based on the mode-coupling theory as

$$q_{\text{max}} = \frac{1}{2.64\xi^+}, \quad (22)$$

where we corrected the original value 2.55<sup>38</sup> to the new value 2.64 according to the recent results of the critical scaling theory.<sup>72</sup>  $\xi^+$  is the correlation length of the supercritical fluid. Since we are dealing with subcritical temperatures, it is more consistent (but numerically equivalent) to reformulate Eq. (22) in terms of  $\xi^-$ , the correlation length of the subcritical fluid,

$$q_{\text{max}} = \frac{1}{5.17\xi^-}. \quad (23)$$

Both correlation lengths obey a scaling law

$$\xi^\pm = \xi_0^\pm |1 - T/T_c|^{-\nu}, \quad (24)$$

where  $\nu = 0.63$  is a critical exponent. Critical amplitudes  $\xi_0^\pm$  in Eq. (24) are related as

$$\frac{\xi_0^+}{\xi_0^-} \simeq 1.96, \quad (25)$$

which explains the mathematical equivalency of Eqs. (22) and (23). Critical amplitude  $\xi_0^+$  can be obtained from another critical scaling ratio

$$\frac{\sigma_0(\xi_0^+)^2}{k_B T_c} \simeq 0.39, \quad (26)$$

where  $T_c$  is the critical temperature. The critical amplitude  $\sigma_0$  for the surface tension has been obtained by fitting scaling relation

$$\sigma = \sigma_0(1 - T/T_c)^{2\nu} \quad (27)$$

to the experimental surface tension data (for the list of data see Appendix B).

Using Eqs. (23) to (27), the bare surface tension in Eq. (21) can be related to the experimental value as

$$\sigma_{\text{bare}} = \sigma_{\text{exp}} \left( 1 + \frac{3}{8\pi} \frac{T}{T_c} \frac{1}{2.72} \right). \quad (28)$$

This is equivalent to the result of Gross,<sup>21</sup> aside from the updated numerical value in the denominator. The effect of the CW is strongest at the critical point, where the bare surface tension is higher by 4.42% than the experimental value, and it remains significant down to the triple point temperature. We note that Eq. (28) is universal, i.e., substance independent.

Eq. (21) assumes an infinitely large system. In a finite system, the maximum CW wavelength is limited by the system's linear dimension. Correspondingly, a lower cutoff of the wave-number  $q_{\text{min}}$  should be considered. This is also the case of the nanodroplets relevant to nucleation. We estimate the maximum wavelength as a half of the circumference of the droplet,

$$\lambda_{\text{max}} = \pi r_s, \quad (29)$$

where radius of the droplet is represented by the radius of the surface of tension,  $r_s$ . This estimate corresponds to the oblate-prolate ellipsoid oscillations, which is the lowest mode of CW on a sphere. The lower cutoff of the wavenumber is then

$$q_{\text{min}} = \frac{2\pi}{\lambda_{\text{max}}} = \frac{2}{r_s}. \quad (30)$$

The critical cluster radius depends on the temperature  $T$  and the supersaturation  $S$ . We evaluated both cutoffs for the experimental nucleation data considered here for the

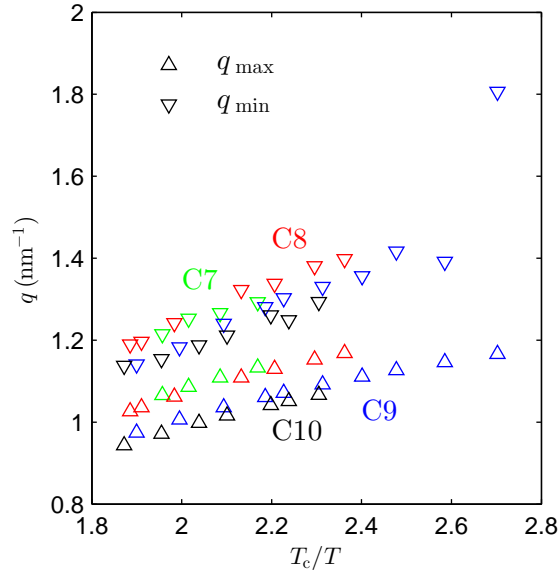


FIG. 1. Minimum cutoff  $q_{\min}$ , Eq. (30), and maximum cutoff  $q_{\max}$ , Eq. (23), of the CW wave numbers as functions of the inverse reduced temperature. Plotted for *n*-heptane (C7), *n*-octane (C8), *n*-nonane (C9) and *n*-decane (C10). The plotted values correspond to experimental nucleation data.

comparison with theoretical predictions (more in Sec. VII). This was done in order to determine the range of the CW wavenumbers relevant for the critical clusters. The upper cutoff  $q_{\max}$  was directly computed for a given temperature  $T$  rounded to a certain value for each series (every individual experiment differed in the temperature somewhat). To evaluate the lower cutoff  $q_{\min}$  using Eq. (30), the radius  $r_s$  was obtained by interpolating the data computed by DGT for the experimental supersaturation  $S_{\text{exp}}$ . For every rounded temperature we got several cutoffs  $q_{\min}$  depending on the supersaturation of the data point; for clarity we considered only the minimal  $q_{\min}$  for given rounded temperature so that the range  $(q_{\min}, q_{\max})$  was the widest possible. Fig. 1 shows both cutoffs for the experimental data computed using Eqs. (23) and (30). The seemingly outlying  $q_{\min}$  point in the upper right corner of Fig. 1 corresponds to data<sup>73</sup> at higher supersaturations and thus smaller critical clusters than the rest. It can be seen that  $q_{\min} > q_{\max}$  in all cases. Therefore, the range  $(q_{\min}, q_{\max})$  is an empty interval; this means that the critical clusters are too small to accommodate any CW. All thermal fluctuations are bulk-like density fluctuations included in the continuous density profile model. Consequently, the bare spherical phase interface

obtained by DGT is an appropriate representation for the critical clusters.

## VI. NUMERICAL METHOD

Eq. (17) with boundary conditions given by Eq. (18) form a boundary value problem. This simply looking problem has several difficulties. First, the density profile near the gaseous phase has a sharp, corner-like, shape; at the gas-phase side, its slope changes abruptly. This “stiff” behavior is caused by the strongly non-linear right-hand side of the differential equation. The second difficulty is that for large droplets the density profile in the interior of the droplet is almost perfectly flat. The difference of the density in the droplet center  $\rho(0)$  to the density  $\rho_L$ , following from the equality of chemical potentials (2), approaches zero rapidly as the droplet becomes large compared to the thickness of the phase interface. This situation occurs for droplets much larger than the typical critical clusters, so that the resulting uncertainty does not influence the nucleation rate computations presented here. However, it represents an obstacle in studying the asymptotic behavior of the size-dependent surface tension when the droplet radius approaches infinity.

In a previous work,<sup>60</sup> the boundary problem was solved using a MATLAB<sup>74</sup> procedure BVP4. This procedure uses a finite difference scheme: the original interval is divided into subintervals, where the right-hand side of differential equation (17) is integrated. An initial approximation of the solution is required. In many general cases, the initial guess can be very crude. However, in case of Eq. (17) with right-hand side computed from a realistic EoS, this initial approximation had to be very close to the final solution to ensure a convergence of the iteration procedure. Due to these problems, this integration procedure was considered as impractical for routine calculations.

To overcome the above mentioned difficulties, a new algorithm was developed based on the simple but robust shooting method. The boundary value problem was converted into an initial value problem by estimating the density in the center of the droplet  $\rho_0$ , so the initial conditions were

$$\rho(0) = \rho_0, \quad \frac{d\rho}{dr}(0) = 0. \quad (31)$$

The initial value problem was then solved using an implementation of the variable-step Runge–Kutta method (MATLAB function ODE45). The original boundary condition in Eq. (18), in theoretical formulation placed to infinity, can be modified to  $\rho(R) = \rho_V$  where  $R$  is

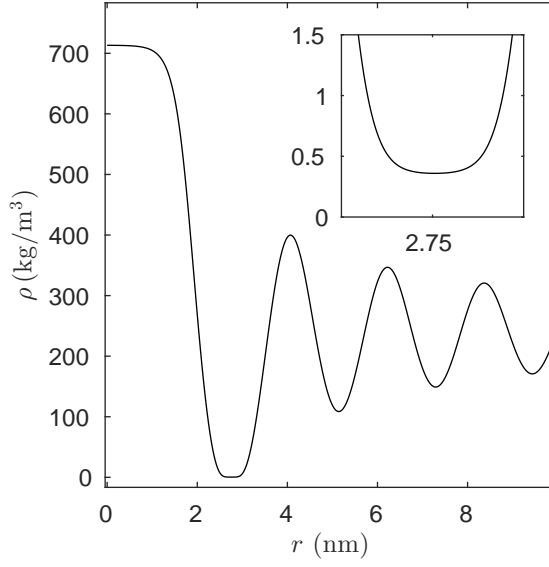


FIG. 2. Density profile  $\rho$  of a critical cluster as a function of distance from the center of the droplet  $r$  for  $n$ -heptane at temperature  $T = 276$  K and supersaturation  $S = 4.4$  computed using the DGT combined with the PC-SAFT EoS. Inset is the detail of the minimum.

finite but sufficiently large, such that the theoretical density profile at  $R$  is sufficiently close to the vapor density. In the shooting method, the center density  $\rho(0)$  is searched for in an iteration procedure such that the right-hand boundary condition is matched.

As shown in Fig. 2, numerical solutions of Eq. (17) with conditions defined by Eq. (31) indicate an oscillatory behavior. In this example, a decrease from a density in the center  $\rho_0 = 713 \text{ kg/m}^3$  down to the vapor density  $\rho_V = 0.36 \text{ kg/m}^3$  occurs within the first 3 nm. Then the curve detaches from the vapor density and oscillates around density  $\rho \simeq 250 \text{ kg/m}^3$ , corresponding to a physically unstable (but numerically stable) solution of the equality of chemical potentials, Eq. (2). This oscillatory behavior was observed for estimates of  $\rho_0$  lying between the correct value and the saturated liquid density  $\rho_L$ . Solutions of Eq. (17) for guesses of  $\rho_0$  slightly below the correct value approached the vapor density and then detached downwards, quickly crossing the zero density. Because of this behavior, enforcing the boundary condition at certain fixed coordinate  $R$  was found impractical. Therefore, the second condition of Eq. (31) was changed to

$$\min_{r < R} \rho(r) = \rho_V. \quad (32)$$

In addition, estimates undershooting the vapor density have been rejected. As a result, the

proper value  $\rho_0$  was approached from above. To achieve a fast convergence, we attempted to compute a next approximation of  $\rho_0$  based on the linear extrapolation of the previous two guesses and the corresponding difference of the left and right sides of Eq. (32). Unfortunately, this modified secant method appeared to be unreliable because the numerical solution of Eq. (17) exhibits a quasi-random error when considered as a function of parameter  $\rho_0$ . The magnitude of this numerical error is small enough so that it does not affect the computations of the work of formation. However, the unsmooth dependence on  $\rho_0$  caused convergence failures for  $\rho_0$  guesses close to the correct boundary value solution. This problem was remedied by changing the secant method to a slower but more robust bisection method. Additional improvements<sup>75</sup> were developed to make the algorithm more robust and precise. In particular, the inner and outer parts of the density profile in intervals where the compressibility only negligibly differs from compressibility at  $\rho_0$  or at  $\rho_V$  were substituted by an analytical solution of a linearized Eq. (17).

## VII. RESULTS AND DISCUSSION

We performed DGT and CNT computations for four alkanes, *n*-heptane, *n*-octane, *n*-nonane, and *n*-decane, for temperatures corresponding to nucleation rate experimental data by Rudek et al.,<sup>76</sup> Hung et al.,<sup>77</sup> Luijten,<sup>78</sup> Viisaanen et al.<sup>79</sup> and Wagner and Strey,<sup>73</sup>

- *n*-heptane (C7): 249 K, 259 K, 268 K, 276 K,
- *n*-octane (C8): 241 K, 248 K, 258 K, 267 K, 287 K, 298 K, 302 K,
- *n*-nonane (C9): 220 K, 230 K, 240 K, 247.6 K, 257 K, 267 K, 272 K, 284 K, 298 K, 313 K,
- *n*-decane (C10): 268 K, 276 K, 281 K, 294 K, 303 K, 316 K, 330 K.

Computations were done using the PC-SAFT EoS and the Peng–Robinson<sup>80</sup> (PR) EoS. Influence parameters  $c$  were computed using Eq. (20) based on the “bare” surface tension of the planar phase interface that was obtained from the experimental surface tension using Eq. (28). (See Appendix B for more information about the experimental surface tension.) The computations of the density profiles for critical clusters were performed using the algorithm described in Sec. VI. The nucleation rates were evaluated using Eq. (9), DGT works of



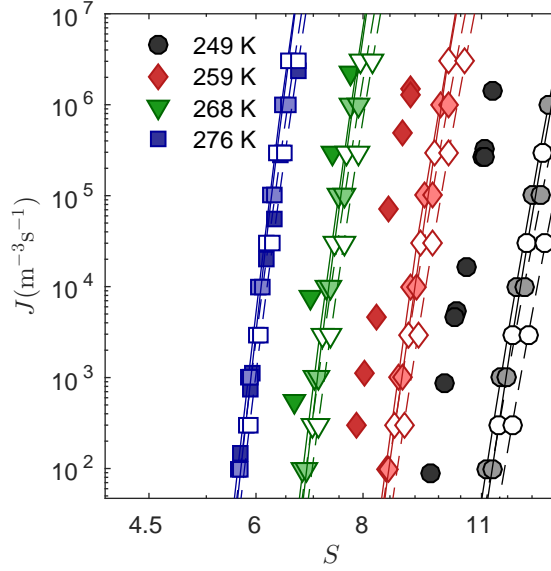


FIG. 3. Nucleation rates  $J$  of  $n$ -heptane as functions of supersaturation  $S$  for various temperatures in logarithmic scale. One color always corresponds to one temperature. Comparison of theoretical nucleation rates, Eq. (9), with experiments by Rudek et al.<sup>76</sup> Solid lines correspond to the DGT, dashed lines to the CNT. Lines with light-color symbols corresponds to the PC-SAFT EoS, with white symbols to the PR EoS. Experimental data are depicted by dark-color symbols.

formation were obtained using Eq. (15) for the computed density profiles, the works of formation for CNT were found using Eq. (10) with  $\sigma = \sigma_\infty$ .

Figs. 3 to 10 show nucleation rates depending on the supersaturations, Eq. (1), computed using the various combinations of DGT and CNT with PC-SAFT and PR EoSs compared with the experimental data. One color and one symbol always correspond to one temperature. Lines depict the theoretical data: solid lines with light-colored symbols are the DGT and PC-SAFT computations, dashed lines with light-colored symbols correspond to CNT and PC-SAFT, solid lines with white symbols to DGT and PR, dashed lines with white symbols to CNT and PR.

The darkest symbols depict the experimental data. It will be discussed that the experiments were not conducted at the same nominal temperatures  $T_0$  shown in the figures as the experimental temperatures  $T_{\text{exp}}$  slightly varied. To enable a direct comparison, the experimental supersaturations  $S_{\text{exp}}$  were corrected to match the nominal temperature. A Taylor expansion was done for  $\ln S_{\text{exp}}$  around the experimental temperature  $T_{\text{exp}}$  to match

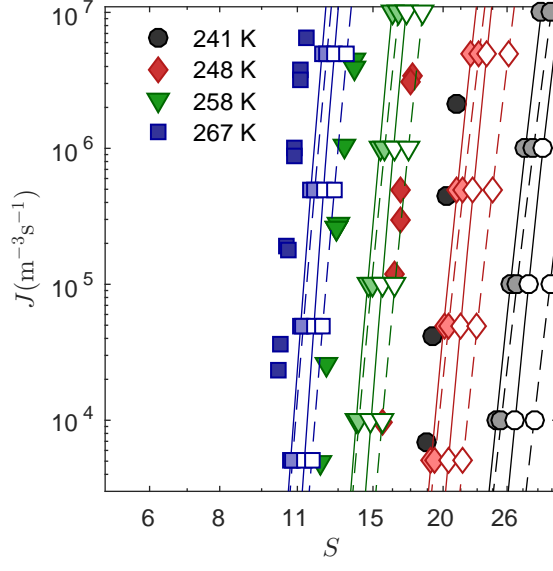


FIG. 4. Nucleation rates  $J$  of  $n$ -octane as functions of supersaturation  $S$  for various temperatures in logarithmic scale. Experimental data are given by Rudek et al.<sup>76</sup> Markers and lines are defined in the same way as in Fig. 3.

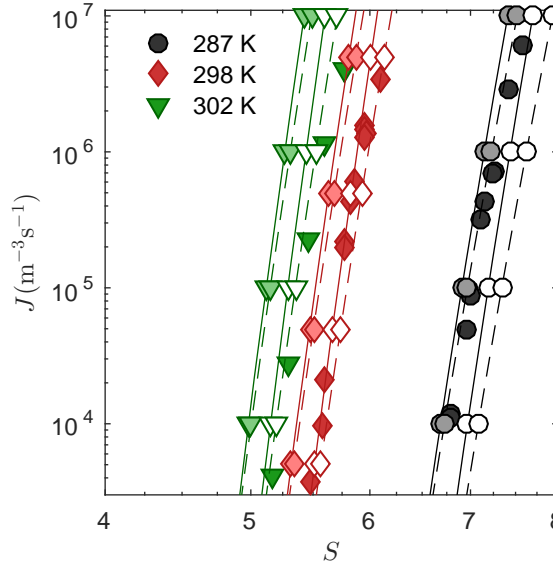


FIG. 5. Nucleation rates  $J$  of  $n$ -octane as functions of supersaturation  $S$  for various temperatures in logarithmic scale. Experimental data are given by Rudek et al.<sup>76</sup> Markers and lines are defined in the same way as in Fig. 3.

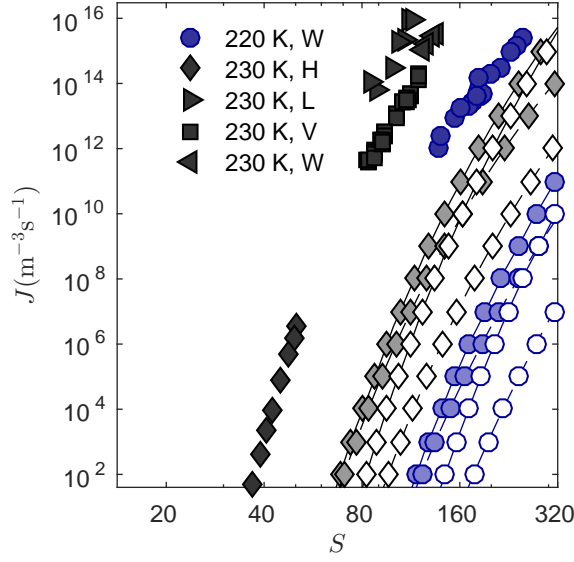


FIG. 6. Nucleation rates  $J$  of  $n$ -nonane as functions of supersaturation  $S$  for various temperatures in logarithmic scale. Experimental data are given by Wagner et al.<sup>73</sup> (W), Hung et al.<sup>77</sup> (H), Luijten<sup>78</sup> (L) and Viisanen et al.<sup>79</sup> (V). Markers and lines are defined in the same way as in Fig. 3.

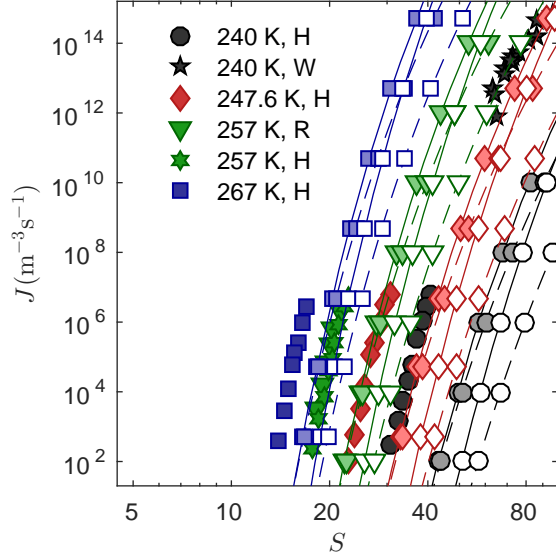


FIG. 7. Nucleation rates  $J$  of  $n$ -nonane as functions of supersaturation  $S$  for various temperatures in logarithmic scale. Experimental data are given by Hung et al.<sup>77</sup> (H), Wagner et al.<sup>73</sup> (W) and Rudek et al.<sup>76</sup> (R). Markers and lines are defined in the same way as in Fig. 3.

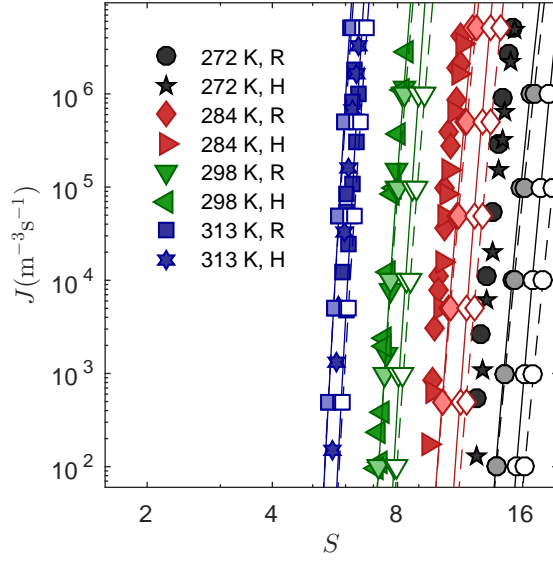


FIG. 8. Nucleation rates  $J$  of  $n$ -nonane as functions of supersaturation  $S$  for various temperatures in logarithmic scale. Experimental data are given by Rudek et al.<sup>76</sup> (R) and Hung et al.<sup>77</sup> (H). Markers and lines are defined in the same way as in Fig. 3.

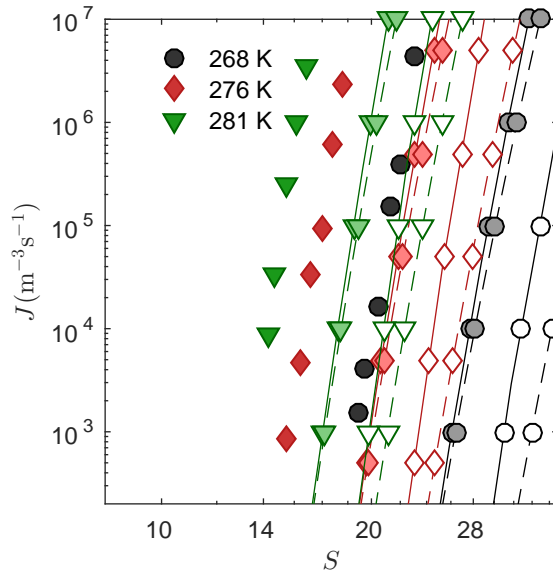


FIG. 9. Nucleation rates  $J$  of  $n$ -decane as functions of supersaturation  $S$  for various temperatures in logarithmic scale. Experimental data are given by Rudek et al.<sup>76</sup> Markers and lines are defined in the same way as in Fig. 3.

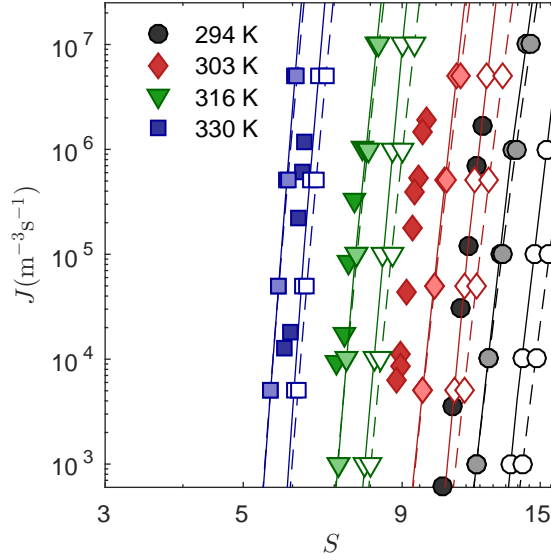


FIG. 10. Nucleation rates  $J$  of  $n$ -decane as functions of supersaturation  $S$  for various temperatures in logarithmic scale. Experimental data are given by Rudek et al.<sup>76</sup> Markers and lines are defined in the same way as in Fig. 3.

the desired temperature  $T_0$ ,

$$\ln S_0 \doteq \ln S_{\text{exp}} + \frac{\partial \ln S}{\partial T}(T_{\text{exp}}, J_{\text{exp}}) \cdot (T_0 - T_{\text{exp}}), \quad (33)$$

where we defined  $S_0 = S(T_0, J_{\text{exp}})$ . However, the derivative  $\partial \ln S / \partial T$  would be difficult to obtain, hence it was substituted by

$$\frac{\partial \ln S}{\partial T} = - \frac{\partial \ln J}{\partial T} \bigg/ \frac{\partial \ln J}{\partial \ln S}. \quad (34)$$

These derivatives were evaluated by differentiating Eq. (9).

The slopes of experimental data with respect to supersaturation relatively well correspond to the theoretical slopes. However, all the lines show a systematic, temperature-dependent shift.

Another way how to compare theoretical predictions with experiments is via mutual ratios of their nucleation rates. Figs. 11 to 13 show ratios of theoretical and experimental nucleation rates corresponding to the experimental temperatures and supersaturations as functions of inversed reduced temperatures. Numerical data were twice interpolated using cubic splines; first,  $\ln J$  was interpolated with respect to  $\ln S$  on two theoretical isotherms neighboring  $T_{\text{exp}}$  such that their  $\ln S$  corresponded to the experimental value  $\ln S_{\text{exp}}$ . Then

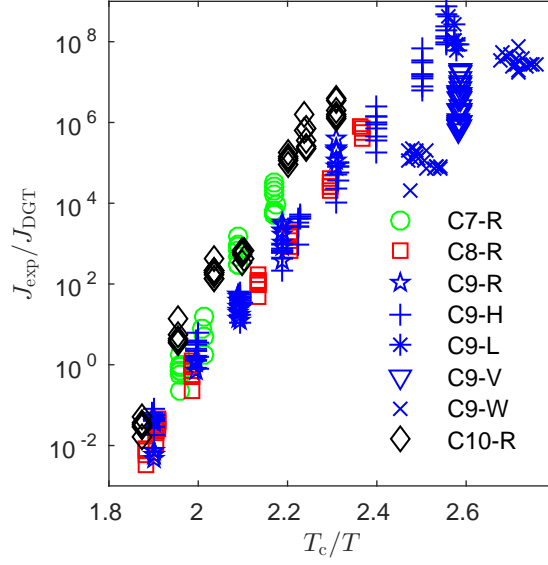


FIG. 11. Ratios of nucleation rates of the selected  $n$ -alkanes computed using the DGT and PC-SAFT EoS and experimental nucleation rates as functions of inverse reduced temperature. Experimental data are given by Rudek et al.<sup>76</sup> (R), Hung et al.<sup>77</sup> (H), Luijten<sup>78</sup> (L), Viisaanen et al.<sup>79</sup> (V) and Wagner and Strey<sup>73</sup> (W).

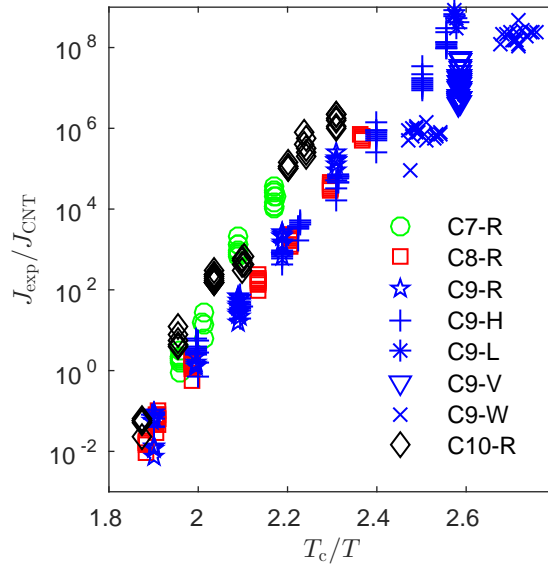


FIG. 12. Ratios of nucleation rates of the selected  $n$ -alkanes computed using the CNT and PC-SAFT EoS and experimental nucleation rates as functions of inverse reduced temperature. Experimental data are defined in the same way as in Fig. 11.

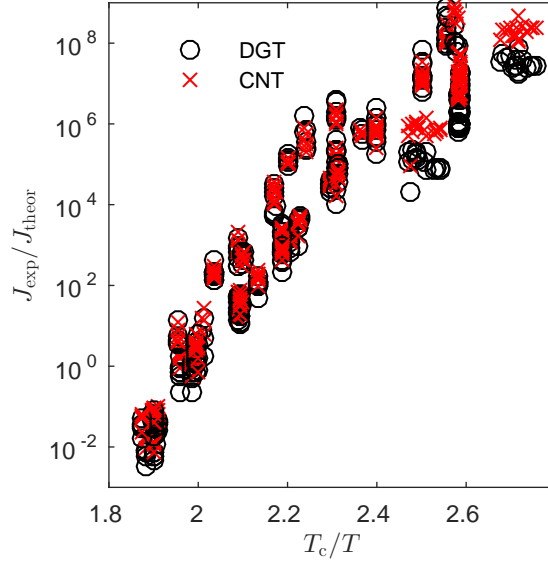


FIG. 13. Ratios of nucleation rates of the selected  $n$ -alkanes as functions of the inverse reduced temperature, comparison of results shown in Figs. 11 and 12.

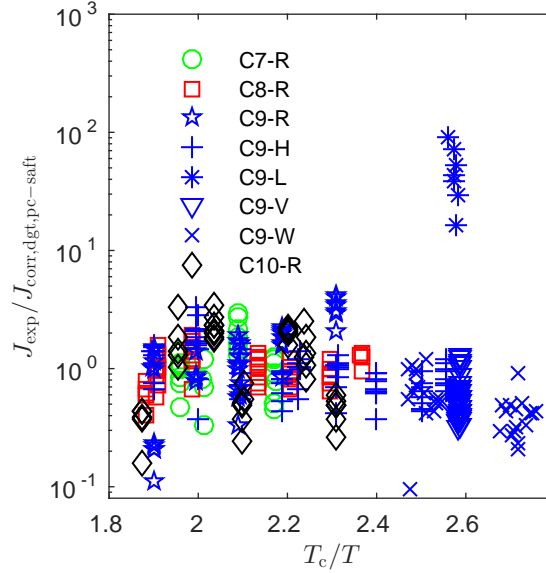


FIG. 14. Ratios of the experimental nucleation rates to DGT with PC-SAFT EoS predictions corrected using correlation, Eq. (36), as a function of the inverse reduced temperature.

these two nucleation rates were again interpolated with respect to temperature to match  $T_{\text{exp}}$ .

Fig. 11 gives the ratios of the experimental nucleation rates to the nucleation rates computed using DGT and PC-SAFT EoS. Fig. 12 shows an analogous comparison of ex-

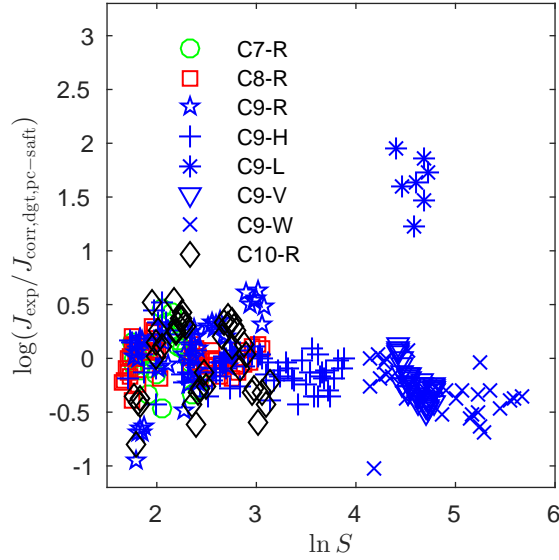


FIG. 15. Ratios of the experimental nucleation rates to DGT with PC-SAFT EoS predictions corrected using correlation, Eq. (36), as a function of supersaturation.

perimental data with CNT. In both figures, one color and one symbol correspond to one experimental data set. Results of DGT with PC-SAFT EoS and CNT with PC-SAFT EoS are compared in Fig. 13.

Clearly, the experimental data show a strong temperature trend which is not predicted by any of the theories. The ratios of experimental to theoretical nucleation rates for the various alkanes appear to follow almost a single linear function of the reciprocal reduced temperature.

$$\ln \left( \frac{J_{\text{exp}}}{J_{\text{theor}}} \right) \simeq A + B \frac{T_c}{T}, \quad (35)$$

where  $A$  and  $B$  are empirical parameters. As discussed by McGraw and Laaksonen<sup>81</sup>, the dependence of the ratio of experimental to theoretical nucleation rates on supersaturation is rather weak; in other words, the dependence of the nucleation rate on the supersaturation is predicted relatively well by the theory. However, some discrepancies can be observed for the data of  $n$ -nonane for which the experiments were done in a wide range of supersaturations. Consequently, we propose an additional term describing the dependence on the supersaturation,

$$\ln \left( \frac{J_{\text{exp}}}{J_{\text{theor}}} \right) \simeq A + B \frac{T_c}{T} + C \ln S. \quad (36)$$

We used the least-squares method to determine the parameters in Eq. (36) for  $n$ -nonane



for both nucleation theories and both EoSs. Except for *n*-nonane, the nucleation rate data for selected *n*-alkanes are available in a rather narrow supersaturation range. This makes it impossible to obtain a reliable value for parameter  $C$ . Therefore, we used the numerical value of coefficient  $C$  for *n*-nonane as an approximation of the supersaturation dependence for other alkanes. Figs. 14 and 15 show the ratios of experimental nucleation rates  $J_{\text{exp}}$  to Eq. (36). These figures show that the correlation successfully captures the variability of the experimental data. Values of coefficients  $A$ ,  $B$  and  $C$  are listed in Tab. I for DGT and CNT combined with PC-SAFT and PR EoSs.

TABLE I. Coefficients of Eq. (36).

PC-SAFT, DGT:	A	B	C
heptane	-110.7738	62.1559	-6.1818
octane	-94.01211	53.1095	-6.1818
nonane	-91.89308	52.5203	-6.1818
decane	-100.6096	58.3962	-6.1818
PC-SAFT, CNT:	A	B	C
heptane	-97.9379	53.8308	-3.7779
octane	-82.0400	45.0167	-3.7779
nonane	-79.5862	44.0546	-3.7779
decane	-88.9715	50.0613	-3.7779
PR, DGT:	A	B	C
heptane	-134.7050	80.0453	-12.0051
octane	-119.4497	73.1246	-12.0051
nonane	-119.5625	75.3177	-12.0051
decane	-130.1146	83.2105	-12.0051
PR, CNT:	A	B	C
heptane	-124.5077	72.4331	-8.7391
octane	-109.2277	65.3503	-8.7391
nonane	-109.5674	67.5294	-8.7391
decane	-119.1090	74.7644	-8.7391

Typically, the experiments provide nucleation rates in a relatively narrow range deter-

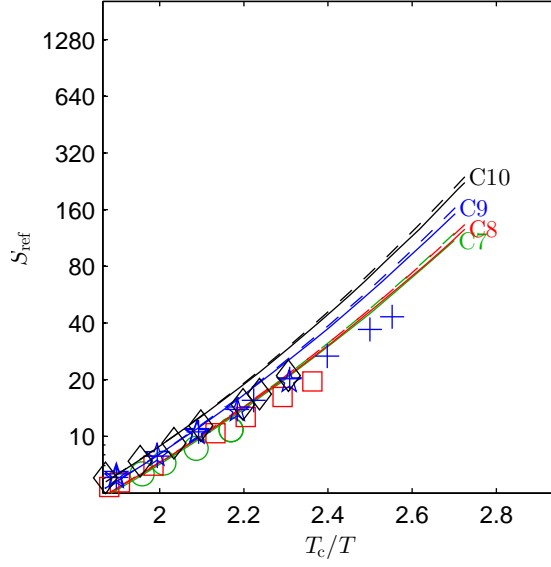


FIG. 16. Dependence of supersaturation  $S$  on the inverse reduced temperature  $T_c/T$  for all four  $n$ -alkanes. They were fitted to one nucleation rate  $J_{\text{ref}} = 7.57 \times 10^4 \text{m}^{-3}\text{s}^{-1}$ . Lines correspond to the DGT data: solid lines to the PC-SAFT EoS, dashed lines to the PR EoS. Symbols depict the experimental data<sup>76,77</sup> (same correspondence as in Fig. 11). One color corresponds to one substance (including experimental data).

mined by the experimental method. Therefore, it is practical to represent the experimental data as a temperature dependence of supersaturation  $S_{\text{ref}}$  corresponding to a chosen reference nucleation rate  $J_{\text{ref}}$ . Figs. 16 and 17 show a temperature dependence of the supersaturation depending on the inverse reduced temperature  $T_c/T$  for all four substances for theoretical data and experiments. Numerical calculations were performed additionally for a wider range of temperatures than what is covered by the experiments to give a better picture of the temperature trend. Experimental data by Rudek et al.<sup>76</sup> and Hung et al.<sup>77</sup> were measured in a substantially lower range of nucleation rates than by Luijten,<sup>78</sup> Viisaanen et al.<sup>79</sup> and Wagner and Strey<sup>73</sup>. For this reason, we used two reference nucleation rates  $J_{\text{ref}} = 7.57 \times 10^4 \text{m}^{-3}\text{s}^{-1}$  and  $J_{\text{ref}} = 3.22 \times 10^{13} \text{m}^{-3}\text{s}^{-1}$  which were obtained as geometrical averages of the nucleation rates included in each data subset.

The experimental data was recorded for various nucleation rates. To reduce it to the reference nucleation rate, the theoretical data were interpolated using a cubic spline. For

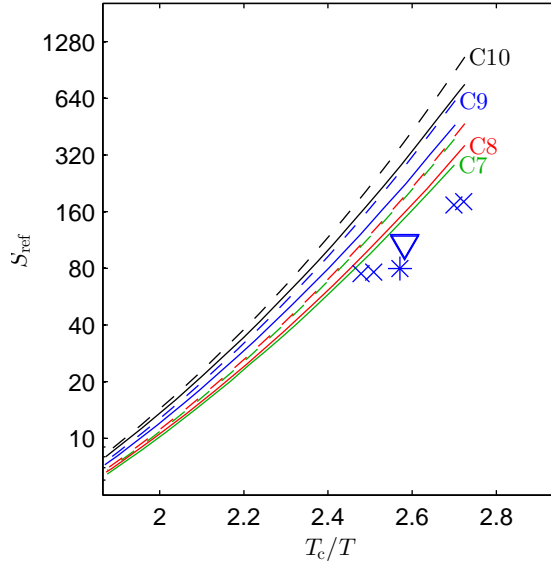


FIG. 17. Dependence of supersaturation  $S$  on the inverse reduced temperature  $T_c/T$  for all four  $n$ -alkanes fitted to nucleation rate  $J_{\text{ref}} = 3.22 \times 10^{13} \text{m}^{-3}\text{s}^{-1}$ . Lines are defined in the same way as in Fig. 16. Symbols depict the experimental data<sup>73,78,79</sup> (same correspondence as in Fig. 11).

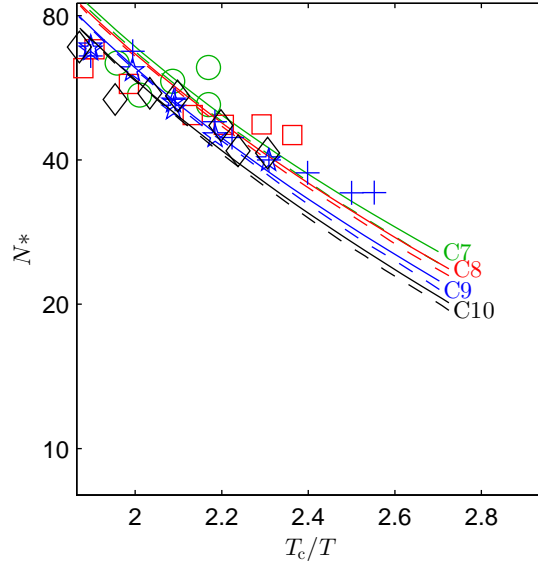


FIG. 18. Dependence of number of molecules in critical cluster  $N^*$  on the inverse reduced temperature  $T_c/T$  for all four  $n$ -alkanes fitted to nucleation rate  $J_{\text{ref}} = 7.57 \times 10^4 \text{m}^{-3}\text{s}^{-1}$ . Lines and experimental data are defined in the same way as in Fig. 16.

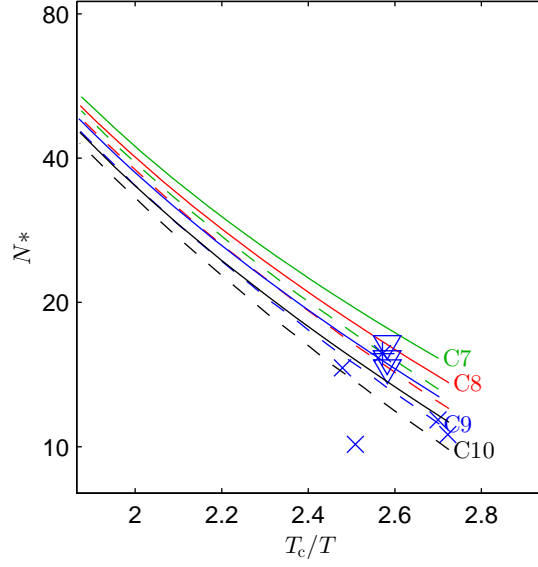


FIG. 19. Dependence of number of molecules in critical cluster  $N^*$  on the inverse reduced temperature  $T_c/T$  for all four  $n$ -alkanes fitted to nucleation rate  $J_{\text{ref}} = 3.22 \times 10^{13} \text{m}^{-3} \text{s}^{-1}$ . Lines are defined in the same way as in Fig. 16, experimental data as in Fig. 17.

experimental data, we assumed a linear dependence,

$$\ln J_{\text{exp}} = b_1 + b_2 \ln S_{\text{exp}}. \quad (37)$$

where coefficients  $b_1$  and  $b_2$  were fitted using the least squares method for each isothermal experimental series. One symbol in Figs. 16 and 17 (and also 18 and 19) corresponds to one isothermal series of measurements, typically including five measurements. Supersaturations  $S$  range from 5.39 to 43.18 for the case of  $J = 7.57 \times 10^4 \text{m}^{-3} \text{s}^{-1}$  (Fig. 16) and from 74.94 to 181.525 for the case  $J = 3.22 \times 10^{13} \text{m}^{-3} \text{s}^{-1}$  (Fig. 17).

Figs. 18 and 19 show a temperature dependence of the number of molecules in the critical cluster  $N^*$  depending on the inverse reduced temperature. Again the data was fitted to match one reference nucleation rate. For GT data, the number of molecules  $N^*$  was evaluated as

$$N^* = \rho_V V_{N^*} + \Delta N_{N^*}, \quad (38)$$

where  $\Delta N_{N^*}$  is the excess number of molecules given by Eq. (19) and  $V_{N^*}$  is the volume of the droplet consisting of  $N^*$  molecules. A rational estimate of volume is the volume of a sphere enclosed by the surface of tension,  $V_{N^*} = 4/3\pi r_{s,N^*}^3$ .

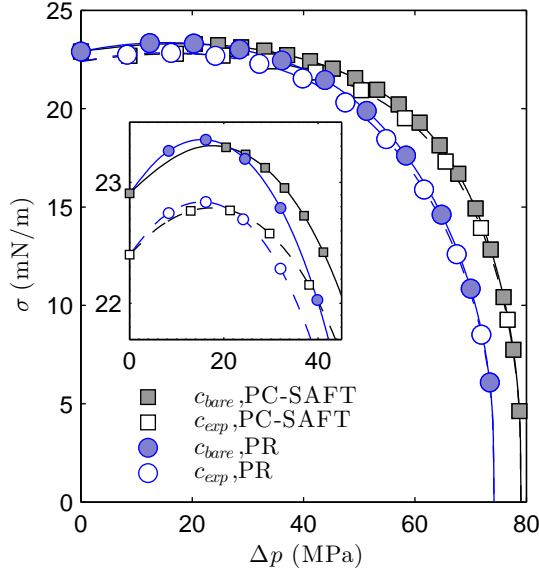


FIG. 20. Surface tensions  $\sigma$  as functions of Laplace pressure  $\Delta p$  of *n*-heptane at temperature  $T = 276$  K. Inset is the detail of the beginning where the lines cross. Lines are results of the DGT computations with PR and PC-SAFT EoS using  $c$  obtained from experimental surface tension  $\sigma_{exp}$ , Eq. (20), and bare surface tension  $\sigma_{bare}$ , Eqs. (20) and (28).

Regarding the experimental data, the number of molecules of the critical cluster was evaluated using the nucleation theorem,<sup>82</sup>

$$\left( \frac{\partial \ln J}{\partial \ln S} \right)_T = N^* + 1. \quad (39)$$

In fact, the derivative has already been fitted by Eq. (37), therefore,  $N^* = b_2 - 1$ .

Again, we split the experimental data into two groups and used  $J_{ref} = 7.57 \times 10^4 \text{m}^{-3}\text{s}^{-1}$  and  $J_{ref} = 3.22 \times 10^{13} \text{m}^{-3}\text{s}^{-1}$  for the reference values. The number of molecules in critical cluster  $N^*$  in Figs. 18 and 19 range from 34.2 to 68.9 for the case of  $J_{ref} = 7.57 \times 10^4 \text{m}^{-3}\text{s}^{-1}$  and from 10.1 to 16.4 for the case  $J_{ref} = 3.22 \times 10^{13} \text{m}^{-3}\text{s}^{-1}$ .

Figs. 16, 17, 18, and 19 show that, despite the large disagreement in terms of the nucleation rate, the theories provide qualitatively correct predictions. However, there is a clear disagreement in the slopes. Predicted derivatives of the supersaturation  $S$  and of the number of molecules in the critical cluster  $N^*$  with respect to temperature at constant nucleation rate differ from the experimental slopes, especially for low temperatures.

As discussed in Sec. V, CW broaden the phase interface and somewhat decrease the resulting surface tension with respect to the bare surface tension corresponding to a phase

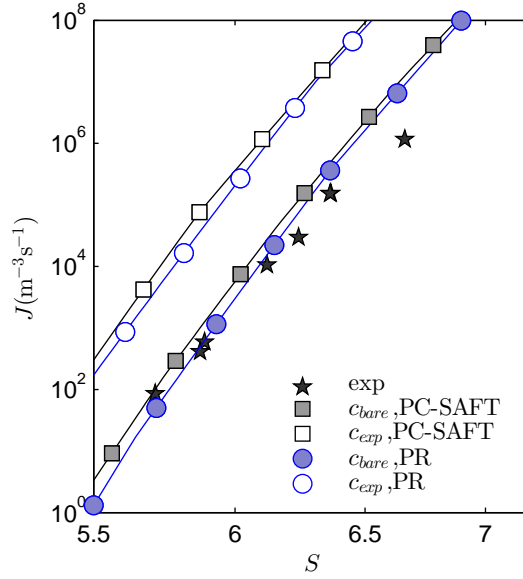


FIG. 21. Nucleation rates  $J$  as functions of supersaturation  $S$  of  $n$ -heptane at temperature  $T = 276$  K. Lines are the same as in Fig. 20. Nucleation rates are also compared to the experimental data by Rudek et al.<sup>76</sup> (black stars).

interface constrained to be free of waves. Fig. 20 shows the surface tension depending on the Laplace pressure  $\Delta p$  computed using DGT, the two EoSs (PR and PC-SAFT), and two different choices of influence parameters. The figure demonstrates an example for  $n$ -heptane at temperature of 276 K. The Laplace pressure is connected with the radius of the droplet  $r$  via Young–Laplace equation, Eq. (11). Therefore,  $\Delta p = 0$  at left corresponds to an infinite radius, i.e., the planar phase interface with surface tension  $\sigma_\infty$ . The size-dependent surface tension was obtained from Eq. (12) based on the work of formation Eq. (15). At the right end, the surface tension according to DGT vanishes at the spinodal. Lines  $c_{\text{bare}}$  connect results for influence parameters computed using Eq. (20), where  $\sigma_\infty$  was cleared of CW using Eq. (28). This is a prediction considered as correct, because, as found in Sec. V, the surface of the critical clusters is practically free of CW and, at the same time, the bare surface tension is the appropriate value to compute the influence parameter because DGT does not include CW. Lines  $c_{\text{exp}}$  correspond to the influence parameters computed via Eq. (20) using the experimental surface tension. This is the standard approach; however, it is considered as less accurate. From Fig. 20 it can be seen that  $\sigma_{\text{bare}} > \sigma_{\text{exp}}$ . The surface tension curves for both EoSs start at either  $\sigma_{\text{bare}}$  or at  $\sigma_{\text{exp}}$  at  $\Delta p = 0$ , but then tends to

a spinodal value given by the particular EoS. The inset figure shows a detail of the trends for low Laplace pressures. The range of Laplace pressures corresponding to the critical clusters in the experiments considered is on the descending branches of the curves close to the maximum. It can be seen that CW have a significant effect on the surface tension. This effect is bigger or at least comparable (in other cases) with the effect of replacing the cubic PR EoS by the sophisticated PC-SAFT EoS. A reason can be seen in an fortuitous crossing of the lines predicted by both EoSs just in the relevant range.

Fig. 21 shows nucleation rates depending on the supersaturation of *n*-heptane at temperature of 276 K. Again, the two EoSs and the two influence parameters were used, similarly as in Fig. 20. The stars depict the experimental data. Constraining the phase interface to be free of CW increasing the surface tension and, consequently, enhances the work of formation and lowers the nucleation rates. The effect is quite large, which proves the importance of such a treatment. We note that the quantitative agreement of the experimental data with the theoretical prediction shown in Fig. 21 is rather fortuitous: due to the strong temperature effect, the differences are larger at other temperatures.

## VIII. CONCLUSIONS

We computed nucleation rates of four alkanes: *n*-heptane, *n*-octane, *n*-nonane, and *n*-decane, using the density gradient theory and the classical nucleation theory. For the calculations, an original algorithm was developed to solve an Euler–Lagrange equation which together with the boundary conditions forms a boundary value problem. Several enhancements of the numerical method were developed to ensure a safe convergence to the proper density profiles. We used a simple cubic Peng–Robinson EoS, which essentially is an empirical modification of the van der Waals EoS, and the PC-SAFT EoS, which is based on molecular arguments.

For computing the nucleation rates, we used an expression based on the classical nucleation theory with corrected supersaturation dependence, Eq. (9). The work of formation was obtained using the density gradient theory or using the Gibbs formula based on the surface tension for the planar phase interface. Comparison of the nucleation rates computed using DGT and CNT with the experiments did not show any qualitative difference. The temperature trend of both theories lacks several effects.

We also studied the effect of CW on the surface tension and the nucleation rates. It was found that in the experimentally relevant range, the critical clusters are so small that the shortest wave-lengths of the CW are already too large to fit to the surface of the nanoscopic droplet representing the critical cluster. This means that the thermal motion of the molecules is completely accounted for in the DGT description. Therefore, for a consistent computation of the works of formation using the DGT, it is necessary to remove the effect of CW. With DGT, this can be achieved in relatively simple manner by fitting the influence parameter to the bare surface tension corresponding to the planar phase interface free of the CW.

Three contributions to the surface tension of a droplet can be recognized in Fig. 20. First is the Tolman’s linear effect which accounts for the mild increase of surface tension (for low  $\Delta p$ ). This effect is related to symmetry properties of the density profile, expressed by the Tolman length. Second, quadratic effect, appears to be decisive in bending the curvature such that the surface tension reaches a maximum and then decreases towards the spinodal. The quadratic effect can be attributed to the finite thickness of the phase interface and to changes in its shape as the critical cluster becomes smaller. Third is the capillary wave effect, which decreases the surface tension of nano-droplets as a part of the spectrum of the CW does not fit to the finite dimensions of the droplet. Suppression of the CW leads to a considerable enhancement of the predicted surface tensions and, in turn, the nucleation rates.

Obviously, DGT represents an important improvement with respect to CNT as it takes into account the finite thickness of the phase interface and a smooth density profile, which is close to realistic. Moreover, accounting for the capillary wave effect turned out to be important. Replacing a cubic-type EoS developed as an empirical correction of the van der Waals equation by a molecular-based modern EoS also brings the simulations closer to reality. However, there still remains an unknown effect preventing quantitative agreement of the theoretical predictions with the experimental data.

## SUPPLEMENTARY MATERIAL

The data points of the figures presented in this article are listed in the supplementary material.



TABLE II. Parameters of the PR EoS

	$T_c$ (K)	$p_c$ (bar)	$\omega(-)$
<i>n</i> -heptane	540.13	27.36	0.3365
<i>n</i> -octane	569.32	24.97	0.3765
<i>n</i> -nonane	594.55	22.81	0.4140
<i>n</i> -decane	617.70	21.03	0.4495

## ACKNOWLEDGMENTS

The research leading to these results has received funding from the Norwegian Financial Mechanism 2009-2014 under Project Contract No. 7F14466, from the Czech Science Foundation grant No. GJ15-07129Y, and from the institutional support RVO: 61388998. Besides, B.P. thanks for a partial support from the grant No. SGS15/215/OHK4/3T/14.

## Appendix A: Parameters of equations of state

For the PC-SAFT EoS, molecular parameters  $m, \sigma$  and  $\epsilon$  for selected *n*-alkanes used in this study were taken from the original work of Gross and Sadowski<sup>62</sup>.

The Peng–Robinson equation is given by

$$p = \frac{\rho R_g T}{1 - b\rho} - \frac{a\alpha\rho^2}{1 + 2b\rho - (b\rho)^2}, \quad (\text{A1})$$

where  $R_g = 8.3144598 \text{ J mol}^{-1} \text{ K}^{-1}$  is the universal gas constant and  $a, b, \alpha$  are Peng–Robinson constants. They are given by

$$\begin{aligned} a &= 0.45724 \frac{R_g^2 T_c^2}{p_c}, \\ b &= 0.0778 \frac{R_g T_c}{p_c}, \\ \alpha &= \left[ 1 + (1 - \sqrt{T/T_c})(0.37464 + 1.54226\omega - 0.26992\omega^2) \right]^2, \end{aligned} \quad (\text{A2})$$

where  $p_c$  is the critical pressure and  $\omega$  is the acentric factor. Acentric factors were used from the work by Lemmon and Goodwin.<sup>83</sup> Critical parameters  $T_c$  and  $p_c$  and acentric factor  $\omega$  for the four *n*-alkanes are listed in Tab. II.

TABLE III. Table of parameters for the fit of the experimental surface tension

	$A$ (mN/m)	$B$ (mN/m)	$C$ (mN/m)
$n$ -heptane	54.1778	-0.7586	3.9897
$n$ -octane	56.5399	-10.4928	8.4723
$n$ -nonane	53.9000	-	-
$n$ -decane	53.6000	-	-

## Appendix B: Experimental surface tension

The influence parameter  $c$  was computed using the experimental surface tension. The experimental values were taken from Jasper et al.<sup>84</sup> for all the selected substances, Grigoryev<sup>85</sup> for heptane (C7) and octane (C8), Voliak and Andreeva<sup>86</sup> for C7 and C8, Rolo et al.<sup>87</sup> for C7 and decane (C10), Okada et al.<sup>88</sup> for C8.

The actual value of surface tension was computed using a temperature correlation. For heptane and octane, we used approach by Somayajulu<sup>89</sup>,

$$\sigma = A\left(\frac{T_c}{T} - 1\right)^{5/4} + B\left(\frac{T_c}{T} - 1\right)^{9/4} + C\left(\frac{T_c}{T} - 1\right)^{13/4}. \quad (\text{B1})$$

For nonane and decane we made our own fit based on the scaling around the critical temperature,

$$\sigma = A\left(\frac{T_c}{T} - 1\right)^{1.26}. \quad (\text{B2})$$

Values of parameters  $A$ ,  $B$  and  $C$  from Eqs. (B1) and (B2) are listed in Tab. III.

## REFERENCES

- <sup>1</sup>R. Becker and W. Dring, Ann. Phys. **24** (1935).
- <sup>2</sup>Y. B. Zeldovich, Zh. Teor. Eksp. Fiz **12**, 525 (1942).
- <sup>3</sup>Y. B. Zeldovich, Acta physicochim. URSS **18**, 1 (1943).
- <sup>4</sup>H. Vehkamäki, *Classical Nucleation Theory in Multicomponent Systems* (Springer, 2006).
- <sup>5</sup>D. Kaschiev, *Nucleation - Basic Theory with Applications* (Butterworth Heinemann, 2000).
- <sup>6</sup>V. Kalikmanov, *Nucleation Theory*, Lecture Notes in Physics, Vol. 860 (Springer Netherlands, 2013).
- <sup>7</sup>B. E. Wyslouzil and J. Wölk, The Journal of Chemical Physics **145**, 211702 (2016).

- <sup>8</sup>T. Němec, Chemical Physics **467**, 26 (2016).
- <sup>9</sup>J. D. van der Waals, Verhandel. Konink. Akad. Weten. **1** (1893).
- <sup>10</sup>J. Rowlinson, J. Stat. Phys. **20**, 200 (1979).
- <sup>11</sup>J. W. Cahn and J. E. Hilliard, J. Chem. Phys. **28**, 258 (1958).
- <sup>12</sup>J. W. Cahn and J. E. Hilliard, J. Chem. Phys. **31**, 688 (1959).
- <sup>13</sup>C. Ebner, W. Saam, and D. Stroud, Physical Review A **14**, 2264 (1976).
- <sup>14</sup>R. Evans, Adv. Phys. **28**, 143 (1979).
- <sup>15</sup>H. Kahl and S. Enders, Fluid Phase Equilibria **172**, 27 (2000).
- <sup>16</sup>H. Kahl and S. Enders, Physical Chemistry Chemical Physics **4**, 931 (2002).
- <sup>17</sup>S. Enders, H. Kahl, and J. Winkelmann, Fluid phase equilibria **228**, 511 (2005).
- <sup>18</sup>S. Enders and H. Kahl, Fluid Phase Equilibria **263**, 160 (2008).
- <sup>19</sup>D. Fu and Y. Wei, Industrial & Engineering Chemistry Research **47**, 4490 (2008).
- <sup>20</sup>D. Fu, H. Jiang, B. Wang, and S. Fu, Fluid Phase Equilibria **279**, 136 (2009).
- <sup>21</sup>J. Gross, J. Chem. Phys. **131** (2009).
- <sup>22</sup>C. Klink and J. Gross, Ind. Eng. Chem. Res. **53**, 6169 (2014).
- <sup>23</sup>C. Klink, B. Planková, and J. Gross, Ind. Eng. Chem. Res. **54**, 46334642 (2015).
- <sup>24</sup>A. Laaksonen and D. W. Oxtoby, The Journal of chemical physics **102**, 5803 (1995).
- <sup>25</sup>G. Wilemski and J.-S. Li, J. Chem. Phys. **121**, 7821 (2004).
- <sup>26</sup>M. Iwamatsu, The Journal of chemical physics **130**, 164512 (2009).
- <sup>27</sup>M. Iwamatsu and Y. Okabe, The Journal of chemical physics **133**, 044706 (2010).
- <sup>28</sup>M. J. McGrath, J. N. Ghogomu, N. T. Tsona, J. I. Siepmann, B. Chen, I. Napari, and H. Vehkamäki, The Journal of chemical physics **133**, 084106 (2010).
- <sup>29</sup>A. Obeidat, M. Gharaibeh, H. Ghanem, F. Hrahsheh, N. Al-Zoubi, and G. Wilemski, ChemPhysChem **11**, 3987 (2010).
- <sup>30</sup>X. Xu, D. E. Cristancho, S. Costeux, and Z.-G. Wang, Soft Matter **9**, 9675 (2013).
- <sup>31</sup>Ø. Wilhelmsen, D. Bedeaux, S. Kjølstrup, and D. Reguera, The Journal of chemical physics **140**, 024704 (2014).
- <sup>32</sup>Ø. Wilhelmsen, D. Bedeaux, and D. Reguera, The Journal of chemical physics **142**, 064706 (2015).
- <sup>33</sup>R. N. Dahms, Journal of colloid and interface science (2014).
- <sup>34</sup>F. P. Buff, R. A. Lovett, and J. F. H. Stillinger, Phys. Rev. Lett. **15**, 621 (1965).
- <sup>35</sup>R. F. Kayser, Phys. Rev. A **33**, 1948 (1986).

- <sup>36</sup>D. Beysens and M. Robert, J. Chem. Phys. **87**, 3056 (1987).
- <sup>37</sup>J. Meunier and D. Langevin, J. Phys. Lettres **43**, 185 (1982).
- <sup>38</sup>J. Meunier, J. Phys. **48**, 1819 (1987).
- <sup>39</sup>M. Napiórkowski and S. Dietrich, Phys. Rev. E **47**, 1836 (1993).
- <sup>40</sup>K. R. Mecke and S. Dietrich, Physical review E **59**, 6766 (1999).
- <sup>41</sup>K. Mecke and S. Dietrich, J. Chem. Phys. **123**, 204723 (2005), arXiv:0505294 [cond-mat].
- <sup>42</sup>a. Doerr, M. Tolan, W. Prange, J.-P. Schlomka, T. Seydel, W. Press, D. Smilgies, and B. Struth, Phys. Rev. Lett. **83**, 3470 (1999).
- <sup>43</sup>C. Fradin, A. Braslau, D. Luzet, D. Smilgies, M. Alba, N. Boudet, K. Mecke, and J. Dailant, Nature **403**, 871 (2000).
- <sup>44</sup>B. Lin, M. Meron, J. Gebhardt, T. Graber, D. Li, B. Yang, and S. A. Rice, Phys. B Condens. Matter **357**, 106 (2005).
- <sup>45</sup>P. Tarazona, R. Checa, and E. Chacon, Phys. Rev. Lett. **99**, 1 (2007).
- <sup>46</sup>T. Hiester, Phys. Rev. E **78**, 061605 (2008), arXiv:arXiv:0812.1707v2.
- <sup>47</sup>E. Chacón and P. Tarazona, Physical review letters **91**, 166103 (2003).
- <sup>48</sup>P. Tarazona and E. Chacon, Phys. Rev. B **70**, 235407 (2004).
- <sup>49</sup>E. Chacon, P. Tarazona, and J. Alejandre, J. Chem. Phys. **125**, 14709 (2006).
- <sup>50</sup>G. S. Boltachev and V. G. Baidakov, Colloid J. **68**, 26 (2006).
- <sup>51</sup>J. S. Rowlinson and B. Widom, *Molecular Theory of Capillarity* (Clarendonpress, 1982).
- <sup>52</sup>L. D. Landau and E. M. Lifshitz, *Statistical physics, part I*, 3rd ed., Vol. 5 (1980) p. 468.
- <sup>53</sup>J. Barrett, J. Phys. Condens. Matter **9**, L19 (1997).
- <sup>54</sup>S. L. Girshick and C.-P. Chiu, J. Chem. Phys. **93**, 1273 (1990).
- <sup>55</sup>J. Hrubý, in *Nucleation and atmospheric aerosols 2004* (Kyoto University Press, 2004) pp. 268–272.
- <sup>56</sup>D. Reguera and H. Reiss, Physical review letters **93**, 165701 (2004).
- <sup>57</sup>W. G. Courtney, The Journal of Chemical Physics **35**, 2249 (1961).
- <sup>58</sup>V. G. Baidakov, S. P. Protsenko, G. G. Chernykh, and G. S. Boltachev, Phys. Rev. E **65** (2002).
- <sup>59</sup>H. T. Davis, *Statistical mechanics of phases. interfaces, and thin films* (Wiley-VCH, Inc., 1996).
- <sup>60</sup>J. Hrubý, D. G. Labetski, and M. E. H. van Dongen, J. Chem. Phys. **127**, 164720 (2007).
- <sup>61</sup>J. Gross and G. Sadowski, Fluid Phase Equilibr. **168**, 183 (2000).

- <sup>62</sup>J. Gross and G. Sadowski, Ind. Eng. Chem. Res. **40**, 1244 (2001).
- <sup>63</sup>W. Chapman, K. Gubbins, G. Jackson, and M. Radosz, Fluid Phase Equilib. **52**, 31 (1989).
- <sup>64</sup>E. A. Müller and K. E. Gubbins, Ind. Eng. Chem. Res. **40**, 2193 (2001).
- <sup>65</sup>S. P. Tan, H. Adidharma, and M. Radosz, Industrial & Engineering Chemistry Research **47**, 8063 (2008).
- <sup>66</sup>V. Vinš and V. Vacek, J. Chem. Eng. Data **54**, 2395 (2009).
- <sup>67</sup>V. Vinš, J. Hrubý, and B. Planková, International Journal of Thermophysics **34**, 792 (2013).
- <sup>68</sup>V. Vinš, J. Hrubý, and B. Planková, EPJ Web of Conferences **25** (2012).
- <sup>69</sup>E. Schäfer, G. Sadowski, and S. Enders, Fluid Phase Equilibria **362**, 151 (2014).
- <sup>70</sup>J. Gross, O. Spuhl, F. Tumakaka, and G. Sadowski, Ind. Eng. Chem. Res. **42**, 1266 (2003).
- <sup>71</sup>A. Grenner, G. M. Kontogeorgis, N. von Solms, and M. L. Michelsen, Fluid Phase Equilib. **258**, 83 (2007).
- <sup>72</sup>M. A. Anisimov and C. E. Bertrand, in *Applied Thermodynamics of Fluids* (The Royal Society of Chemistry, 2010).
- <sup>73</sup>P. E. Wagner and R. Strey, J. Chem. Phys. **80**, 5266 (1984).
- <sup>74</sup>MATLAB, *version R2015a*, The Mathworks, Inc., Natick, Massachusetts, USA (2010).
- <sup>75</sup>B. Planková, *Mathematical modeling of spherical phase interfaces in real fluids*, Master's thesis, CTU FNSPE (2011).
- <sup>76</sup>M. M. Rudek, J. A. Fisk, V. M. Chakarov, and J. L. Katz, J. Chem. Phys. **105** (1996).
- <sup>77</sup>C.-H. Hung, M. J. Krasnopolter, and J. L. Katz, J. Chem. Phys. **90** (1989).
- <sup>78</sup>C. Luijten, *Nucleation and Droplet Growth at High Pressure*, Ph.D. thesis, Technische Universiteit Eindhoven (1998).
- <sup>79</sup>Y. Viisanen, P. E. Wagner, and R. Strey, J. Chem. Phys. **108**, 4257 (1998).
- <sup>80</sup>D.-Y. Peng and D. B. Robinson, Ind. Eng. Chem., Fundam., **15**, 59 (1976).
- <sup>81</sup>R. McGraw and A. Laaksonen, Phys. Rev. Lett. **76**, 5754 (1996).
- <sup>82</sup>D. W. Oxtoby and D. Kashchiev, J. Chem. Phys. **100**, 7665 (1994).
- <sup>83</sup>E. W. Lemmon and A. Goodwin, Journal of Physical and Chemical Reference Data **29**, 1 (2000).
- <sup>84</sup>J. J. Jasper, E. R. Kerr, and F. Gregorich, J. Am. Chem. Soc. **75**, 5252 (1953).

- <sup>85</sup>B. A. Grigoryev, B. V. Nemzer, D. Kurumov, and J. Sengers, *Int. J. Thermophys.* **13** (1992).
- <sup>86</sup>L. D. Voliak and L. Andreeva, *Zh. Fiz. Khim.* **XXXV**, 1416 (1961).
- <sup>87</sup>L. I. Rolo, A. I. Caco, A. J. Queimada, I. M. Marrucho, and J. A. P. Coutinho, *J. Chem. Eng. Data* **47**, 1442 (2002).
- <sup>88</sup>M. Okada, M. Hattori, T. Ohtake, and K. Watanabe, *Heat Trans. Japanese Res.* **19**, 681 (1990).
- <sup>89</sup>G. R. Somayajulu, *Int. J. Thermophys.* **9**, 559 (1988).